

## Chapter 2

# Chlorine-Terminated Silicon(111) Surfaces

The contents presented in this chapter are based on Cao, P.G., Yu, H.B. and Heath, J.R. "Scanning tunneling microscopy and spectroscopy of wet-chemically prepared chlorinated Si(111) surfaces," *J Phys Chem B*, 110, 23615-23618 (2006). (Ref.<sup>1</sup>)

### 2.1 Introduction

Functionalization of Silicon(111) surfaces with covalently bonded organic reagents has received an increasing interest as a method for tailoring the chemical and electrical properties of Si surfaces.<sup>2-6</sup> In particular, alkyl passivated Si(111) surfaces prepared through a two-step chlorination/alkylation route<sup>4-6</sup> have shown low charge-carrier surface recombination velocities, oxidation resistance in air and during anodic current flow in electrochemical cells, and a number of other interesting chemical and electronic properties. The chlorinated Si(111) surface (Cl/Si(111)) is a key intermediate in this chemistry. Chemical component analysis of Cl/Si(111) surfaces has been performed using X-ray photoelectron spectroscopy,<sup>6,7</sup> infrared,<sup>8</sup> and high-resolution electron energy loss spectroscopy,<sup>9</sup> indicating formation of the Cl-Si bond. The expected 1×1 structure of the chlorination layer was confirmed in a recent scanning tunneling microscopy study of Cl/Si(111) surface prepared by the gas phase reaction of H/Si(111) with molecular chlorine.<sup>9</sup> Cl-Si bond-induced stacking faults were previously observed by Itchkawitz et al.<sup>10</sup> That report was based upon the observation that inequivalent crystallographic

directions ( $\langle\bar{1}\bar{1}2\rangle$  and  $\langle 11\bar{2}\rangle$ ) were found to exhibit the same bilayer step edge structure. In addition, significant enhancement of surface conductance for Cl/Si(111) was reported by Lopinski et al.<sup>11</sup> A p-type inversion layer was used to interpret this effect in terms of the formation of a 2D hole gas.

The morphology of a chlorinated Si(111) surface is apparently dependent upon the nature of the chemistry utilized for that chlorination, and that is the hypothesis that we test in this chapter. For example, when a H/Si(111) surface that is characterized by a low density of step edges is halogenated via the reaction with gas phase molecular chlorine, the resultant Cl/Si(111) surface remains extremely flat.<sup>9</sup> However, when a similarly flat H/Si(111) is chlorinated via the reaction with  $\text{PCl}_5$  in chlorobenzene solution and subsequently alkylated, the resultant alkyl/Si(111) is characterized by a high density of etch pits, with a corresponding large fraction of alkylated Si atoms residing at the edge of those pits.<sup>12, 13</sup> Those atoms are more chemically accessible than the alkylated Si atoms that reside on terraces, and so can play a role in subsequent chemical processes on the surface.<sup>14</sup> They can also play important roles in driving the formation of a stacking fault.<sup>12</sup>

The etch pits presumably originate during the chlorination procedure. In this chapter, we present detailed results on the scanning tunneling microscopy (STM) and tunneling spectroscopy (STS) investigations of wet-chemically prepared Cl/Si(111) surfaces. We show that this wet-chemical chlorination of H/Si(111) does, in fact, introduce a large density of etch pits of one or more atomic steps in depth. Nevertheless, Cl atoms still passivate 100% of the atop Si atom sites on the unreconstructed Si(111) surface. The etch pits result in fragmented  $\langle 11\bar{2}\rangle$  steps and do not lead to stacking faults

on the chlorinated surface. Unlike the case for H/Si(111), methyl/Si(111) or ethyl/Si(111),<sup>15</sup> tunneling spectroscopy revealed the absence of a band gap: current-voltage traces exhibited a non-zero slope at zero applied bias, implying a non-zero density-of-states (DOS) at the Fermi level.

## **2.2 Wet-chemical preparation of Cl-terminated Si(111) surfaces**

The substrates utilized were (111)-oriented, Sb-doped, n-type Si wafers with a low miscut angle of  $\pm 0.5^\circ$  and a resistivity of 0.005-0.02 ohm·cm. Anhydrous inhibitor-free tetrahydrofuran (THF,  $\geq 99.9\%$ , water content  $< 0.002\%$ ) was purchased from Sigma-Aldrich. Phosphorus pentachloride ( $\text{PCl}_5$ , 99.998%) was purchased from Alfa Aesar. These reagents were used as supplied and stored in a glovebox purged with nitrogen.

Silicon wafers were cut into samples of  $0.5 \times 1$  cm pieces. A standard RCA cleaning process was then carried out. Briefly, the substrate was immersed in a basic peroxide solution which is composed of 1:1:4 by volume of 28%  $\text{NH}_3 \cdot \text{H}_2\text{O}(\text{aq})/30\% \text{H}_2\text{O}_2/\text{H}_2\text{O}$  at  $80^\circ\text{C}$  for at least 10 min and then rinsed thoroughly in running Milli-Q water. H-terminated Si(111) surface was then formed after immersing the cleaned sample in 40%  $\text{NH}_4\text{F}$  for about 15 min. This step produces large, atomically flat terraces.<sup>16</sup> Chlorination was performed in a nitrogen-purged glovebox. A few grains of benzoyl peroxide were added to a saturated solution of  $\text{PCl}_5$  in chlorobenzene and the solution was then heated to  $90\text{-}100^\circ\text{C}$  for 50 min. For lower temperature experiments, reaction time was adjusted so that a complete chlorination of the Si surface was reached. This was monitored by the surface conductivity test, since the conductivity was observed to increase significantly in comparison with H/Si. After the reaction, the sample was

removed from the solution and rinsed thoroughly with tetrahydrofuran. The samples were then dried under streaming  $N_2(g)$ , mounted onto a sample stage, and quickly introduced into an Omicron low-temperature STM system.

The STM microscope is contained in an ultrahigh vacuum chamber with an operating pressure of  $<6 \times 10^{-11}$  Torr. Both topographic and spectroscopic data were acquired at 77 K by use of a mechanically cut or etched Pt-Ir tip. In a typical topographic imaging measurement, the tip is brought 5-15 Å away from the sample surface. In our measurements, a tip/vacuum/sample junction resistance of 5-20 GΩ was maintained by setting up the sample voltage and tunneling current. Surface electronic properties are examined by measuring the tunneling spectroscopy simultaneously with topographic image acquisition. Briefly, at each topographic raster scanning point the feedback was temporarily switched off, and the tip-sample distance was then fixed. The tip-sample tunneling current  $I_t$  was then recorded while scanning the tip-sample voltages, which results in a total number of  $\sim 2500$  current-voltage  $I_t(V)$  traces in an STM image. The derivative  $dI_t/dV$  is then numerically calculated from the averaged  $I_t(V)$  spectroscopic data.

### 2.3 STM results

Figure 2.1(a)-(c) shows constant-current STM images of the Cl/Si(111) surfaces prepared at three temperatures. The etch hillocks of a single bilayer step are clearly seen, and are pointing to the  $\langle \bar{1}\bar{1}2 \rangle$  orientation. In comparison with the H/Si(111),<sup>16</sup> an obvious increase in etch pit density was observed for Cl/Si(111) prepared at all three temperatures. These etch pits are of one or more bilayer steps in depth. Previous results

from methylated and ethylated Si(111) surfaces displayed a similar etch pit morphology,<sup>6</sup> although again with atomically flat terraces. The conclusion is that the increased etch pit density is most certainly caused by the wet-chemical chlorination procedure. Since the step sites are expected to be more chemically accessible than the terrace sites, the chlorination chemistry essentially transforms these relatively inert terrace sites to more reactive step sites that can be exploited in subsequent chemical reactions. It may thus be possible to tailor the surface chemical activity by changing the terrace-to-step site ratio via control over the chlorination chemistry. The etching chemistry could, in fact, be modified by changing the reaction temperature (Figure 2.1). The coverage of etch pit and edge atom were quantified and plotted versus temperature in Figure 2.1(d). An increase in reaction temperature led to an increase in both etch pit coverage and terrace-to-step ratio. A dependence of etch pit density upon the reaction conditions was also observed for Cl/Si(111) prepared via reactions of H/Si(111) with Cl<sub>2</sub>(g). Under UV irradiation and at room temperature, Lopinski and coworkers<sup>11</sup> prepared Cl/Si(111) surfaces with a considerable number of etch pits by reaction with molecular chlorine, whereas the reaction without UV irradiation resulted in a completely flat surface with few etch pits.<sup>9</sup> The surface morphology is apparently dependent upon the relative etch rates of the terraces, step edges, kinks and other surface structures. The large number of etch pits in the Cl/Si(111) surface observed on surfaces prepared at higher temperatures is likely ascribable to the increased ratio of the terrace etch rate to the kink etch rate.

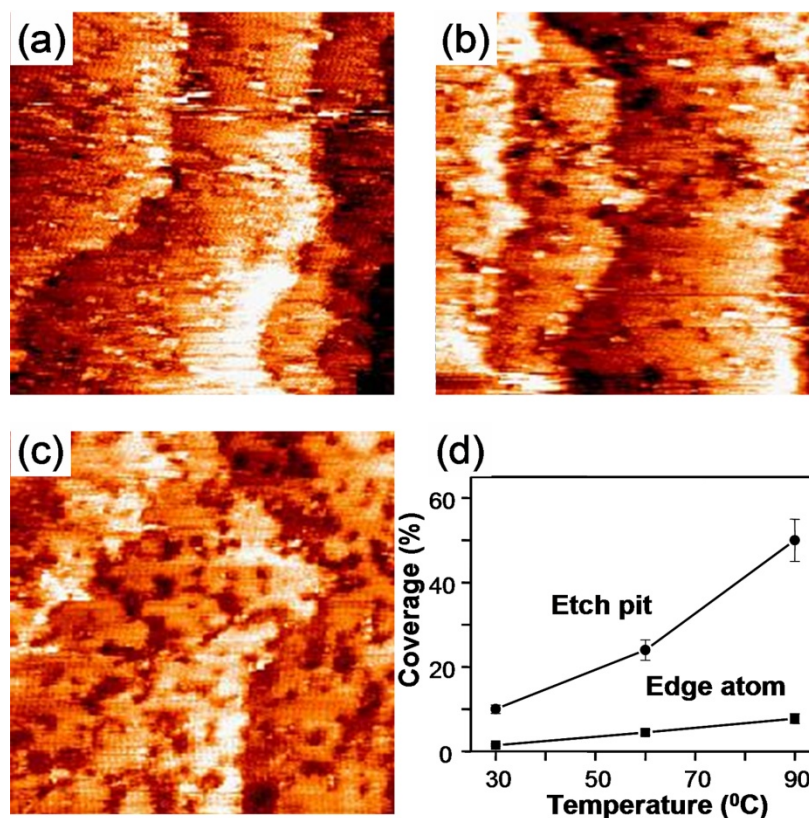


**Figure 2.1. Large-field view of STM topographic images.** (a)-(c) Constant-current STM images of the Cl/Si(111) surfaces prepared at different temperatures - (a) 30°C, 5 hr, (b) 60°C, 3hr, (c) 90°C, 50 min - acquired at a sample voltage of -1.0 V. Scan area is 100 nm × 100 nm for all three images. (d) Plot of etch pit and edge atom coverage against reaction temperature.

In spite of the increased number of etch pits in the chlorinated surface, a full coverage of Cl-Si on the Si(111) atop sites could be achieved through the solution phase chemical approach. This nearly 100% coverage is suggested by the constant-height atomic-resolution image as shown in Figure 2.2, and by experiments in which methyl and acetyl Grignard reagents have been shown to fully alkylate such a chlorinated surface.<sup>6, 14</sup> Constant-current mode images, at this resolution, were of slightly poorer quality but still revealed the full coverage and hexagonal structure of the Cl-Si on the surface. While it

would have been interesting to obtain an image of a step edge at a similarly high resolution to that presented in Figure 2.2, such an image would require constant-current-mode imaging. Statistical analysis of the nearest-neighbor-atom distances revealed a peak value of  $3.90 \pm 0.12 \text{ \AA}$ , which is in agreement with the distance between silicon atop sites on the unreconstructed Si(111) surface.<sup>17</sup> This suggests an unreconstructed  $1 \times 1$  structure and hence a full passivation of the Si atop sites by Cl, consistent with reported results from the gas phase chlorination of H-terminated Si(111).<sup>9</sup> Similar images were obtained from other terrace sites. Atomically flat surfaces with a minimal amount of contamination can be identified from the image, indicating that the wet-chemically prepared Cl/Si(111) can survive at least moderate post-processing conditions that include a several minute air exposure prior to introduction into the UHV STM chamber.

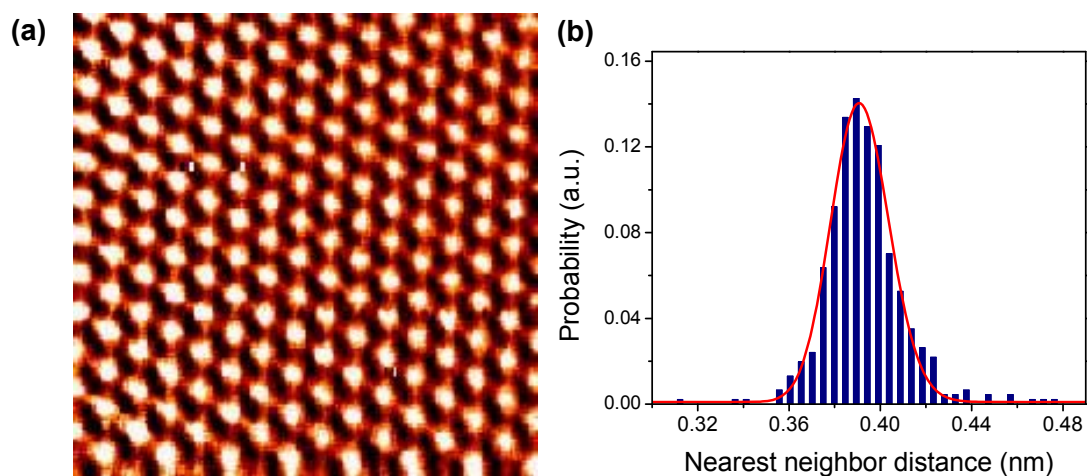


**Figure 2.2. Close-up STM images with atomic resolution.** (a) Constant height STM image of surface prepared at  $90^\circ\text{C}$  showing uniform Cl atom coverage of the atop sites of the unreconstructed surface. Scan area =  $5 \times 5 \text{ nm}$ ,  $V_b = -0.8 \text{ V}$ ,  $I_t = 0.27 \text{ nA}$ . (b) Histogram of the distribution of distance between nearest neighbor atoms. A lognormal fit is indicated by a red line, which peaks at  $0.39 \text{ nm}$ . The full-width at half maximum gives an error of about  $\pm 0.012 \text{ nm}$ .

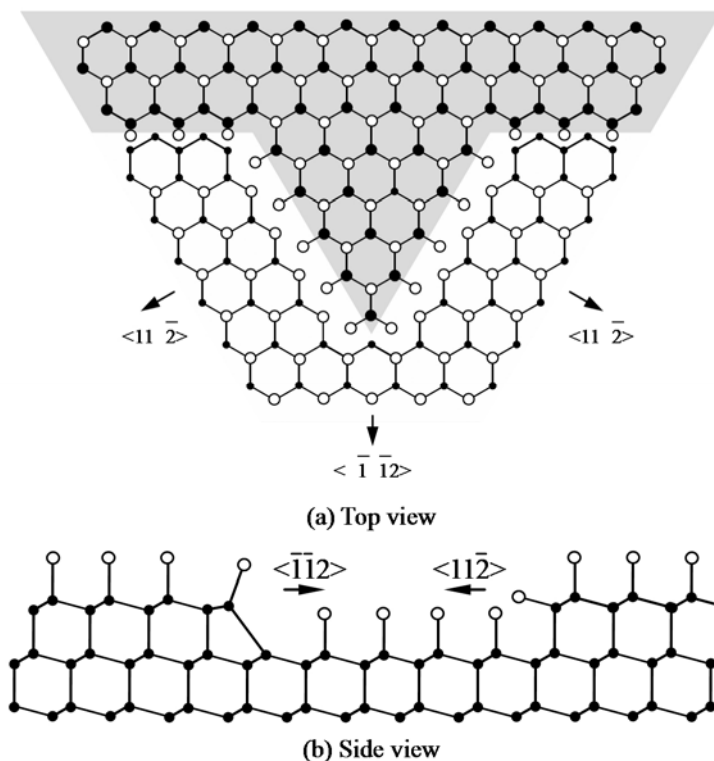


**Figure 2.3. Schematics of the structure of steps on Cl-terminated Si(111) surfaces.**

The  $\langle 11\bar{2} \rangle$  and  $\langle \bar{1}\bar{1}2 \rangle$  steps are indicated by arrows.

Another interesting set of observations are the fragmented  $\langle 11\bar{2} \rangle$  steps with the outward normal along the  $\langle \bar{1}\bar{1}2 \rangle$  orientation. Figure 2.3a is an illustration of the etch hillock observed in STM images. For H/Si(111) surfaces, it has been shown that a  $\langle 11\bar{2} \rangle$  step is terminated by the lower Si atoms of the bilayer, forming a horizontal monohydride termination structure.<sup>16</sup> By contrast,  $\langle \bar{1}\bar{1}2 \rangle$  steps are terminated by the upper Si atoms, resulting in a vertical dihydride structure.<sup>16</sup> Upon chlorination, a rebonded step geometry was formed at the  $\langle \bar{1}\bar{1}2 \rangle$  steps, where the step terminating Si atoms are bonded to the bottom terrace silicon atoms (see Figure 2.3b).<sup>10</sup> The full chlorination of the  $\langle 11\bar{2} \rangle$  step terminating Si atoms has been shown to be energetically unfavorable. This might be attributed to the significant electrostatic repulsion between the negatively charged

chlorine atoms along the upper and lower terraces of the  $\langle 11\bar{2} \rangle$  steps.<sup>10</sup> Periodic DFT calculations indicated that the Si-Cl bond on  $\langle \bar{1}\bar{1}2 \rangle$  is 0.58 eV stronger than on  $\langle 11\bar{2} \rangle$ . For  $\text{CH}_3/\text{Si}(111)$  the difference is even greater (0.67 eV).<sup>12</sup>

A stacking fault basically switches a  $\langle 11\bar{2} \rangle$  step to a  $\langle \bar{1}\bar{1}2 \rangle$  step. Calculations indicated that a full stacking fault on the terraces is energetically possible for etched  $\text{CH}_3/\text{Si}(111)$  and  $\text{Cl}/\text{Si}(111)$  surfaces. Partly faulted regions were observed by Itchckawitz et al.<sup>10</sup> on the  $\text{Cl}/\text{Si}(111)$ , and were inferred for  $\text{CH}_3/\text{Si}(111)$  by us through a combination of experiment<sup>6</sup> and theory.<sup>12</sup> For our  $\text{Cl}/\text{Si}(111)$  surfaces prepared at 90°C, the terrace-to-step site ratio (estimated to be  $\sim 13$  from the STM images) indicates that stacking faults would be energetically possible.<sup>12</sup> However, no stacking faults were observed for any of our preparations. Careful inspection of the etch hillock edges (Figure 2.1c) revealed that the  $\langle 11\bar{2} \rangle$  step edges were actually segmented, or further etched. An etched  $\langle 11\bar{2} \rangle$  step edge site creates two kink sites, each of which possesses the  $\langle \bar{1}\bar{1}2 \rangle$  step edge structure. This further etching therefore partially removes the  $\langle 11\bar{2} \rangle$  step edge atoms and essentially changes the  $\langle 11\bar{2} \rangle$  step structure to the  $\langle \bar{1}\bar{1}2 \rangle$  step structure, thus stabilizing the surface.

## 2.4 STS results

We also investigated the tunneling spectroscopy of wet-chemically prepared  $\text{Cl}/\text{Si}(111)$ . Current-voltage  $I_t(V)$  traces, averaged over the area shown in Figure 2.2a are represented in Figure 2.4a, together with a similarly averaged trace collected from  $\text{H}/\text{Si}(111)$ . The derivative  $dI_t/dV$ , which is roughly proportional to the local density of states, is shown in Figure 2.4b. The set points for bias voltage and current were

experimentally varied to optimize image quality. For the data shown in Figure 2.4a, the parameters were -0.8 V and 0.27 nA for Cl/Si(111) and -1.7 V and 0.12 nA for H/Si(111).

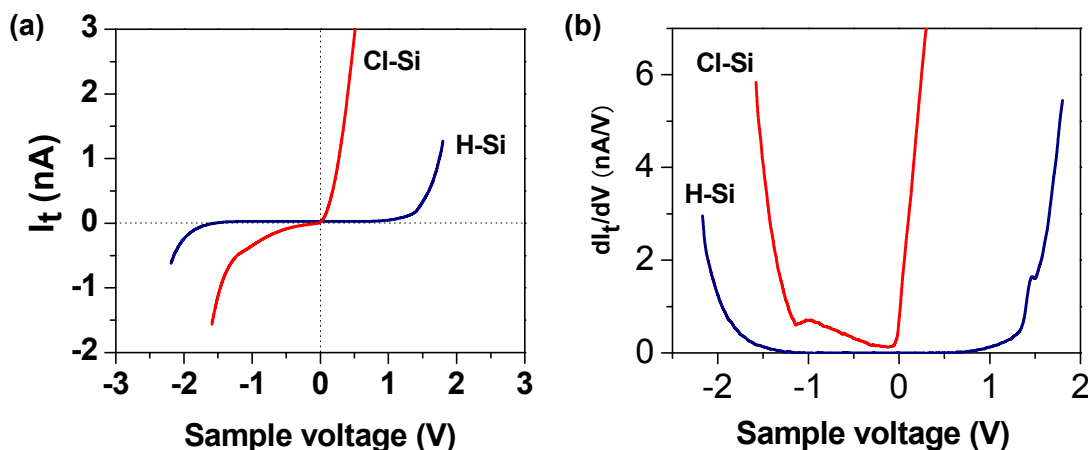


**Figure 2.4. Scanning tunneling spectroscopy of Cl/Si(111).** (a) Representative low temperature (77K) I-V spectra for H- and Cl-terminated Si(111) surfaces. (b) Corresponding  $dI_t/dV$  tunneling spectrum for the above two surfaces.

Fully passivated H/Si(111) exhibits a large conductance gap, and this was observed in a bias voltage range down to -1.7 V, where a limiting value of 1.6 V was obtained. Similarly large conductance gaps have been recently reported for methyl/Si(111) (100% passivation) and ethyl/Si(111) (80% ethyl-; 20% H-passivation).<sup>15</sup> This has been attributed to the absence of surface states for these chemically functionalized surfaces. The apparent larger value of the measured band gap compared to the standard bulk silicon gap (1.12 eV at 300 K) can be attributed to the tip-induced band bending (TIBB, see Figure 2.5a).<sup>18</sup> Since only part of the sample-tip voltage is applied across the vacuum gap, the onset of current is postponed till larger voltage values are reached. Interestingly, at small negative sample voltages just below the sample Fermi level, the expected tunneling current component ( $I_D$ ) from the conduction-band electrons was not observed,

while this is commonly observed at cleaved n-type GaAs surfaces.<sup>19</sup> The absence of this current component suggests a rather small tunneling transmission coefficient of conduction-band electrons from the sample to the tip. A possibility may be that the very sharp tip may not accommodate those states with non-zero momentum parallel to the semiconductor sample surface.<sup>20</sup>

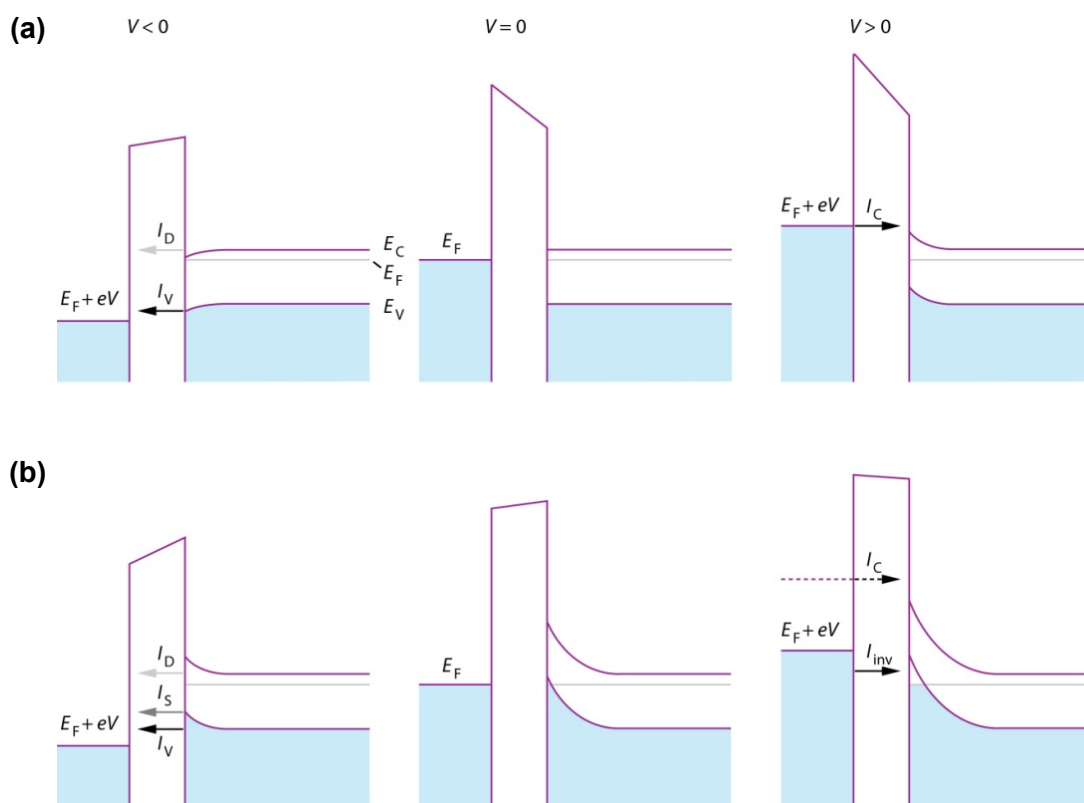


**Figure 2.5. Schematic illustration of energy bands**, showing the conduction-band minimum  $E_C$  and valence-band maximum  $E_V$ . The Fermi level of the sample is denoted by  $E_F$  and that of the tip  $E_F + eV$ , where  $V$  is the sample voltage. (a) Tip-induced band bending (TIBB). The arrows indicate the tunneling direction of electrons. (b) Adatom-induced band bending. The residue TIBB is also indicated at non-zero sample-tip voltages.

The current-voltage characteristics of Cl/Si(111) exhibited no evidence of a band gap (see Figure 2.4a), with the I-V curve possessing a finite slope at zero bias voltage. Varying the bias voltage in a range of  $-1.5 \sim -0.3$  V showed consistent results. This indicates a non-zero DOS at the Fermi level. From the  $dI_t/dV$  versus voltage plot (Figure 2.4b), three different conductance regions are noticed. At positive values of sample voltage, a conductance response attributable to tunneling out of filled levels of the tip and into the empty levels of Si is observed. At negative-valued sample voltages below about  $-1.1$  V the current is dominated by the tunneling of the valence band electrons from the silicon into the tip. The third region is that which is bracketed by negative-valued sample biases between 0 and  $-1.1$  V.

Since the UHV STM images show atomically flat surfaces with minimal surface contamination, the finite conductance observed at zero bias could then be explained in terms of the intrinsic Cl/Si(111) surface properties. Unlike the H/Si(111) where the Fermi level is unpinned, the strong electronegativity of chlorine is expected to induce a large upward band bending (Figure 2.5b), where the Fermi level approaches the top of the valence band edge.<sup>21</sup> Strong surface band bending induced by adsorbates such as metal and semiconductor atoms, oxygen and halogens have been observed at even sub-monolayer coverages.<sup>22</sup> These adsorbates have also been shown to induce intrinsic surface states, pinning the Fermi level ( $E_F$ ) at a position dependent upon the difference between the electronegativity of the adsorbate and the substrate atoms.<sup>22</sup>  $E_F$  pinning close to the edge of the valence band has been previously observed on Cl/GaAs(110) surfaces.<sup>21</sup> Recently, four-point measurements on Cl/Si(111) by Lopinski et al.<sup>11</sup> showed a high surface conductance, which is about 3 times of the bulk value. A p-type inversion

layer was invoked to explain this effect. According to this model, at small positive voltages above the Fermi level, tunneling of electrons into the inversion layer may dominate the current till the onset of the conduction-band current (Figure 2.5b). At small negative sample bias, tunneling of both conduction-band electrons and surface valence-band edge electrons may both contribute to the current. The probability of thermionic emission of silicon conduction-band electrons followed by tunneling through the vacuum barrier is expected to be rather low.<sup>23</sup> At increasing values of negative sample bias, the surface barrier decreases and hence the tunneling current increased. A theoretical model of this surface would likely provide clarification of this picture. Surface recombination velocity measurements<sup>24</sup> have revealed a low velocity for a freshly prepared Cl/Si sample, followed by a sharp increase in recombination rate upon oxidation. Interestingly, although the observation of finite conductance between 0 and -1.1 V may obscure the observation of the valence band edge, the present data do exhibit a gap voltage difference that is very close to the bulk band gap value.

## 2.5 Conclusion

In this chapter, we have reported on the scanning tunneling microscopy and spectroscopic studies of Cl-terminated Si(111) surfaces. Cryo-STM images of wet-chemically prepared Cl/Si(111) surfaces showed an unreconstructed  $1\times 1$  structure and hence full replacement of hydrogen by chlorine atoms. An increased etch pit density relative to gas phase prepared Cl/Si(111) was observed, and could be controlled experimentally. Such control may enable the tailoring of the surface chemical reactivity toward subsequent alkylation and other functionalization processes. Tunneling spectroscopy revealed a non-zero DOS near zero applied bias, in contrast to analogous

measurements on H/Si(111), methyl/Si(111), and ethyl/Si(111) surfaces. This may indicate that the electronegative Cl atoms are inducing surface states which are contributing to current observed within the usual forbidden region.

## 2.6 References

1. Cao, P.G., Yu, H.B. & Heath, J.R. Scanning tunneling microscopy and spectroscopy of wet-chemically prepared chlorinated Si(111) surfaces. *J Phys Chem B* **110**, 23615-23618 (2006).
2. Buriak, J.M. Organometallic chemistry on silicon and germanium surfaces. *Chem Rev* **102**, 1271-1308 (2002).
3. Weldon, M.K., Queeney, K.T., Eng, J., Raghavachari, K. & Chabal, Y.J. The surface science of semiconductor processing: gate oxides in the ever-shrinking transistor. *Surf Sci* **500**, 859-878 (2002).
4. Bansal, A. et al. Alkylation of Si surfaces using a two-step halogenation Grignard route. *J Am Chem Soc* **118**, 7225-7226 (1996).
5. Royea, W.J., Juang, A. & Lewis, N.S. Preparation of air-stable, low recombination velocity Si(111) surfaces through alkyl termination. *Appl Phys Lett* **77**, 1988-1990 (2000).
6. Yu, H.B. et al. Low-temperature STM images of methyl-terminated Si(111) surfaces. *J Phys Chem B* **109**, 671-674 (2005).
7. Rivillon, S. et al. Chlorination of hydrogen-terminated silicon(111) surfaces. *J Vac Sci Technol A* **23**, 1100-1106 (2005).
8. Rivillon, S., Amy, F., Chabal, Y.J. & Frank, M.M. Gas phase chlorination of hydrogen-passivated silicon surfaces. *Appl Phys Lett* **85**, 2583-2585 (2004).
9. Eves, B.J. & Lopinski, G.P. Formation and reactivity of high quality halogen terminated Si(111) surfaces. *Surf Sci* **579**, L89-L96 (2005).
10. Itchkawitz, B.S., McEllistrem, M.T. & Boland, J.J. Equivalent step structures along inequivalent crystallographic directions on halogen-terminated Si(111)-(1x1) surfaces. *Phys Rev Lett* **78**, 98-101 (1997).
11. Lopinski, G.P. et al. Enhanced conductance of chlorine-terminated Si(111) surfaces: Formation of a two-dimensional hold gas via chemical modification. *Phys Rev B* **71**, 125308 (2005).

12. Solares, S.D. et al. Chlorination-methylation of the hydrogen-terminated silicon(111) surface can induce a stacking fault in the presence of etch pits. *J Am Chem Soc* **128**, 3850-3851 (2006).
13. Yu, H.B. et al. Scanning tunneling microscopy of ethylated Si(111) surfaces prepared by a chlorination/alkylation process. *J Phys Chem B* **110**, 23898-23903 (2006).
14. Rohde, R.D., Agnew, H.D., Yeo, W.S., Bailey, R.C. & Heath, J.R. A non-oxidative approach toward chemically and electrochemically functionalizing Si(111). *J Am Chem Soc* **128**, 9518-9525 (2006).
15. Yu, H.B., Webb, L.J., Heath, J.R. & Lewis, N.S. Scanning tunneling spectroscopy of methyl- and ethyl-terminated Si(111) surfaces. *Appl Phys Lett* **88**, 252111 (2006).
16. Hines, M.A. In search of perfection: Understanding the highly defect-selective chemistry of anisotropic etching. *Annu Rev Phys Chem* **54**, 29-56 (2003).
17. Waltenburg, H.N. & Yates, J.T. Surface-chemistry of silicon. *Chem Rev* **95**, 1589-1673 (1995).
18. Mcellistrem, M., Haase, G., Chen, D. & Hamers, R.J. Electrostatic sample-tip interactions in the scanning tunneling microscope. *Phys Rev Lett* **70**, 2471-2474 (1993).
19. Stroscio, J.A., Feenstra, R.M. & Fein, A.P. Local state density and long-range screening of adsorbed oxygen-atoms on the GaAs(110) surface. *Phys Rev Lett* **58**, 1668-1671 (1987).
20. Jager, N.D., Weber, E.R., Urban, K. & Ebert, P. Importance of carrier dynamics and conservation of momentum in atom-selective STM imaging and band gap determination of GaAs(110). *Phys Rev B* **67**, 165327 (2003).
21. Troost, D., Koenders, L., Fan, L.Y. & Monch, W. Pinning of the Fermi level close to the valence-band top by chlorine adsorbed on cleaved GaAs(110) surfaces. *J Vac Sci Technol B* **5**, 1119-1124 (1987).
22. Monch, W. Virtual gap states and Fermi level pinning by adsorbates at semiconductor surfaces. *J Vac Sci Technol B* **4**, 1085-1090 (1986).
23. Stroscio, J.A. & Feenstra, R.M. Scanning tunneling spectroscopy of oxygen adsorbates on the GaAs(110) surface. *J Vac Sci Technol B* **6**, 1472-1478 (1988).
24. Lewis, N.S. Private communication.